

Modeling of Complementary (Void) Plasmon Waveguiding

Eyal Feigenbaum and Meir Orenstein

(Invited Paper)

Abstract—Plasmonic circuit elements, which are based on complementary waveguide structures (waveguides with a dielectric core and metal cladding), are becoming preferred plasmonic devices for applications. In this paper, we look into the modeling of such devices, namely 1-D waveguides and related elements as well as 2-D slots, trenches, and channels supporting plasmonic slow waves. Methods such as the effective index, finite-difference time domain, finite elements, or other full-vectorial propagation schemes are among the methods discussed, and their limitations in the field of plasmonics are set. We believe that although many successful validated modeling methods were presented intensive efforts are still required for perfecting the various tools to faithfully describe nanosized plasmonic wave propagation on high-contrast nanometal discontinuities.

Index Terms—Integrated optics, optical interconnections, optical planar waveguide components, optical propagation, optical propagation in absorbing media, optical propagation in dispersive media, optical propagation in plasma media, optical waveguide components, optical waveguide theory, plasmons.

I. INTRODUCTION

SURFACE plasmon-polariton (SPP)-based waveguides have been a subject of intensive research during the past few years [1]–[5]. Research on them has been focused on the understanding of the benefits and limitations of plasmonic-based circuitry for signal delivery [2], [6] and sensing [1], [7].

The embedded mechanism for all SPP-based waveguiding phenomena is the existence and propagation of a single SPP [8], [9] (to be denoted here as plasmon for brevity) on the interface between regular and negative dielectrics (e.g., metal at optical frequencies). This electromagnetic wave propagating along the single interface with its supporting surface plasma is a slow wave, i.e., smaller phase velocity, shorter wavelength, higher momentum, and higher wave impedance compared to regular waves in the same medium. This effect is the essence of the ability of realizing nanocircuitry based on plasmons. However, this merit does not come without limitation; the accompanying loss is substantial and is further enhanced whenever the slow-wave characteristic is enhanced. This intrinsically limits the propagation length of the plasmonic wave to the range

of about a few micrometers up to a few millimeters (typically), and this is a limitation with substantial impact on the optimized way of exploiting plasmons in circuitry.

The logical extension of the single surface plasmon is the metal film plasmon [10], [11], which supports two plasmonic modes that can be interpreted as the in- and antiphase coupled single surface plasmons, mediated by the metal film. The two-mode degeneracy is removed when the metal thickness is reduced to the order of the skin depth at the given frequency (typically sub-100 nm). The antisymmetrical mode evolves to the so-called long-range SPP (LRSP) [12], which exhibits the longest propagation length in the plasmon family due to smaller overlap with the metal core. Taking a further step toward realization, 2-D rectangular metal waveguides were analyzed by various methods, including the method of lines, effective index (EI) method, coupled dipole equations, and Green dyadic method, and were subsequently verified by experimental measurements [13]–[19]. These strip waveguides were predicted to exhibit LRSP when embedded in a highly symmetrical cladding in addition to other special modes such as corner modes [13]. Asymmetry, which is unavoidable in real devices, reduces the propagation length substantially and leads to a cutoff of the mode when the lateral size of the metal core is of about one wavelength [20], [21]. Circular configuration (metal wires) was analyzed analytically, and it supports various plasmonic modes, some with angular momentum [22]–[25]. The rectangular metallic waveguides were the infrastructure for many theoretical and experimental realizations of plasmonic circuit elements. The LRSP modes of micrometric wide (and nanometric thick) rectangular metal waveguides were measured for asymmetric [14], [26] and symmetric [15], [17] cladding by employing various source-waveguide coupling (e.g., near-field scanning optical microscopy [27], end-fire [15], [17], prism [14], [26], discontinuity [28], and gratings [29]). A large set of related waveguide devices was analyzed, designed, and measured including bends, branches, couplers [18], [30], [31], tapers [14], multimode interference [18], and gratings [32].

Although a good understanding and validation of metal core-based plasmonic waveguides and devices were established, the emphasis was shifted in recent years toward the complementary structure, such as a scheme comprised of dielectric core with plasmonic metal cladding [10], [33], which is the subject of this paper. The motivation for this transition is partially discussed here. While LRSP modes of metal core

Manuscript received May 1, 2007.

The authors are with Technion—Israel Institute of Technology, Haifa 32000, Israel (e-mail: eyalf@tx.technion.ac.il; meiro@ee.technion.ac.il).

Color versions of one or more of the figures in this paper are available online at <http://ieeexplore.ieee.org>.

Digital Object Identifier 10.1109/JLT.2007.903558

waveguides are propagating for up to a few millimeters, their modal transverse dimension is similar to modes of regular dielectric waveguides (few micrometers), so the rationale of using such lossy waveguides (and related devices) for applications is questionable. Furthermore, the transition to nanomodal size in metal core waveguides, although theoretically feasible, requires a very symmetric dielectric cladding and is accompanied by a very short propagation length. The complementary structure is mitigating some of these deficiencies. First, the transverse modal dimension is determined by the dielectric core thickness (penetration to the metal is always about the skin depth). This allows the designer to generate an accurate mode with dimensions that can go to the nanoscale. Since no radiation modes are supported by the (1-D) complementary structure, waveguides and devices can be spaced as close as 150 nm (for typical parameters) with no crosstalk. Due to the absence of the radiation modes, the asymmetry of the surrounding (substrate versus superstrate) does not impact the mode, which is inclosed between the metal layers. Furthermore, the complementary configuration allows the employment of a variety of core materials overlapping optimally with the field intensity profile and can exhibit a span of usable optical characteristics, e.g., nonlinear medium, analyte for sensing, and electrooptic material.

It may look surprising (to the nonexpert) that both a structure and its complementary one support bound modes, which is of course not the case for regular dielectric waveguides. In the latter, although inverse structures were designed for different applications, they do not support bound modes (e.g., hollow fiber [34] and antiresonant reflecting optical waveguides [35] are supporting only leaky modes, and in the more recent dielectric slot waveguide configuration [36], the mode is generated by the finite-width high-index “cladding,” and the slot only enhances the field locally). In the plasmonic case, however, the basic mode is the single interface plasmon, and the plasmonic modes of the complementary structures can be interpreted (as aforementioned) as the two coupled single interface plasmons mediated by the dielectric buffer.

It should be mentioned that another popular field, i.e., the enhanced transmission via hole/slit arrays [1], [37], is highly related to the subject of this paper due to the fact that the transmission is performed eventually through a (short) complementary waveguide as well as due to the mechanisms of efficient harvesting of the input field serving an important role also for our waveguide devices and couplers, as will be discussed.

As the last introductory remark, we believe that waveguide modeling methods and their adaptation to plasmonic circuitry, particularly at the nanoscale, are still in progress and far from being exhausted. A few major obstacles hindering the analysis of plasmonic structures are given as follows: 1) The materials are characterized by extreme dispersion and very high loss; 2) nanodimensions, e.g., edge guiding, require complex computational meshes and special source coupling; and 3) extreme dielectric contrast at the metal dielectric boundaries challenges difference-based method stability, bidirectional power flow (source coupling), etc.

In this paper, we look at various modeling avenues exploited for the research of complementary plasmonic wave-

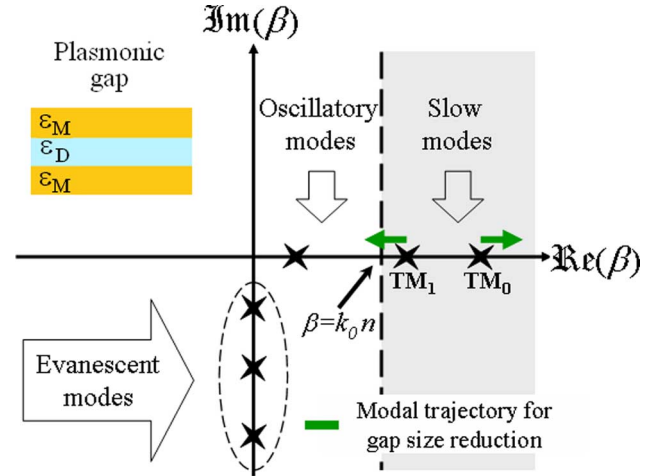


Fig. 1. Modal solutions of plasmonic gap, which is schematically illustrated in the inset, on the complex β plane (propagation constant). Green arrows illustrate the trajectories of the TM_0 and TM_1 modes as the gap width is reduced or the frequency is increased.

guides. This paper is organized by the phenomena studied rather than the modeling methods. We start with 1-D gap (metal–dielectric–metal) plasmon waveguides and related devices and continue to the more diverse 2-D field of plasmonic channel (void carved in metal), slot (cut through thin metal), and trench (cut through thick metal). Finally, we look at the frontier of nanocavities and plasmonic nonlinear devices. We made our best to prepare a comprehensive paper, but due to limited space, not all contributions could be included.

II. PLASMONIC GAP WAVEGUIDES (1-D)

A. Modeling Metal, Dispersion Relations, and Reduced Diffraction Subspaces

The modes of a uniform plasmonic gap waveguide (metal–insulator–metal as depicted in the inset of Fig. 1) can be derived analytically, and the modeling part of this section is related more to the complexity of the metal description. We examine the gap modal structure by employing a metal permittivity model, which is gradually enhanced toward a realistic description. The basic modal features (“Fano modes”) are obtained by the conventional practice of employing the lossless Drude model, while the lossy Drude model and the actual empirical dispersion of typical metals are adding and modifying modal characteristics.

1) *Lossless Drude Model, Closed Waveguide, and the “fate” of a Mode:* The lossless Drude model [10] based on free electron gas yields a metal dielectric constant of the form $\epsilon = \epsilon_0(1 - \omega_p^2/\omega^2)$, where ϵ_0 is the vacuum permittivity, ω is the frequency, and ω_p is the plasma frequency. The compatibility of this model with measurements of typical metals (Au, Ag, Al) [38], [39] is well established for light wavelength above ~ 600 nm, which is remote from the interband transition resonances. For this red–near-IR regime, the electrical permittivity is highly negative, e.g., $\epsilon_{Au}(\lambda = 1550 \text{ nm}) = -131(+12i)$ [38] and is further increasing (absolute value) with wavelength. Due to the highly (negative) dielectric constant, the field penetration to the metal is small, the modes have some

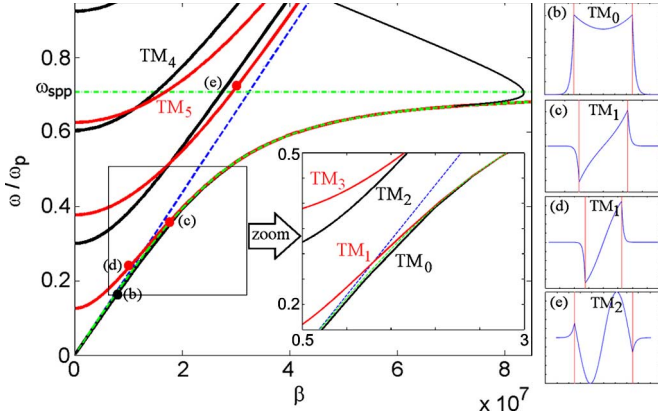


Fig. 2. “Plasmonic gap” dispersion curve of TM modes. The 500-nm gap filled with air ($\epsilon_d = 1$) and the metal are modeled by lossless Drude model with 137-nm plasma wavelength (e.g., for Au or Ag). TM modes: (Black) even and (red) odd; (blue dashed) light line; (green dashed) single surface SPP dispersion curve to the band gap when metal losses are considered. Inset: Enlarged view of dispersion curve, where TM_1 crosses the light line. Modal H_y -field profiles at points (b)–(e) on the dispersion curve are depicted on the right. Metal interfaces are denoted by red lines $\lambda = 1.5 \mu\text{m}$.

similarity to those of a perfect electric conductor (PEC)-cladded waveguide, and the first plasmonic TM mode is similar to the TEM mode (longitudinal E-field becomes very small) of a parallel plate transmission line (TL) [40]. Thus, many modeling tools from the field of TLs can be employed here, as exemplified later [41]. The dispersion relations of the gap plasmonic waveguide are essentially the geometrical dispersion of a dielectric slab with the embedded chromatic dispersion of the metal layers and were derived many times to yield expressions [33] for symmetric and antisymmetric guided modes.

1) Symmetric guided modes:

$$\text{Plasmon : } \tanh(k_p d) = -(k_m/\epsilon_m)/(k_p/\epsilon_d) \quad (1-a)$$

$$\text{Oscillatory : } \tanh(k_O d) = (k_m/\epsilon_m)/(k_O/\epsilon_d) \quad (1-b)$$

2) Antisymmetric guided modes:

$$\text{Plasmon : } \text{ctgh}(k_p d) = -(k_m/\epsilon_m)/(k_p/\epsilon_d) \quad (1-c)$$

$$\text{Oscillatory : } \text{ctg}(k_O d) = -(k_m/\epsilon_m)/(k_O/\epsilon_d) \quad (1-d)$$

where $k_p^2 = \beta^2 - k_0^2 \epsilon_d$, $k_O^2 = k_0^2 \epsilon_d - \beta^2$, and $k_m^2 = \beta^2 - k_0^2 \epsilon_m$.

The complete analysis of the gap plasmonic waveguide (Figs. 1–3) yields two decoupled TE/TM mode families (each family is comprised of three E- and H-field components). It might come as a surprise that although the plasmonic metal is a (negative) dielectric and not a PEC, the modal structure is similar to that of a closed waveguide, such that only a discrete spectrum of bound and evanescent modes is supported (Fig. 1), while the continuous radiation mode spectrum and the complex leaky modes that are so typical of dielectric slab waveguides are both absent. The importance of the absence of radiation modes is obvious for the practical employment of this structure, as well as for more compact modeling of gap waveguide devices.

To better comprehend the modal characteristics, we digress to the single metal interface TM plasmonic mode (green dashed

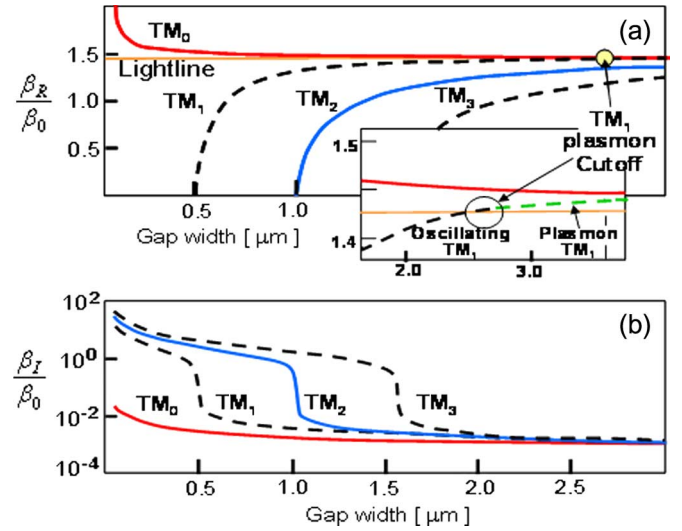


Fig. 3. (a) Real and (b) imaginary parts of propagation constants of some TM modes in plasmonic gap versus the gap width. The inset shows the cutoff region of the asymmetric plasmon mode. The metal is modeled by the Drude model (from [50]) $\lambda = 1.5 \mu\text{m}$, $\epsilon_d = 1.5^2$.

line in Fig. 2). The dispersion curve is asymptotic to the light line at low frequencies and to the SPP frequency ω_{SPP} at high frequencies. Above the ω_{SPP} , a band gap exists up to the plasma frequency ω_p , where the plasmonic modes are absent. For high-frequency plasmons, the longitudinal and transverse E-field components become comparable as well as the dielectric and metal skin depth. The mode becomes substantially slow; the propagation constant and vertical k -component are comparable, which can be modeled as a “retardation-free” case.

The potential plasmonic (slow) modes of the gap waveguide are only the two first TM modes, while all other modes (both higher TM and all TE modes) are either oscillatory or evanescent. It should be emphasized that although the gap is comprised of two metal–dielectric interfaces, we cannot interpret simply the two first TM modes as in- and antiphase coupling of the two single surface SPP modes, particularly for narrow (below one wavelength) gaps, where the coupling coefficient is very large (this interpretation is, however, valid for a metal slab of any thickness). This is evident by examining the trajectory of mode TM_1 (Figs. 1–3). As the thickness of the gap is decreased below about one wavelength, the TM_1 plasmonic (slow) wave crosses the light line and becomes an oscillatory (fast) wave, and eventually at a thickness of about half-wavelength, this mode crosses the cutoff point to become an evanescent one. TM_1 exhibits an additional extraordinary feature. For very thin gaps, the cutoff frequency approaches ω_p such that the modal dispersion curve enters the band gap and exhibits a negative slope, i.e., TM_1 becomes a backward wave mode [10].

The TM_0 mode is a pure plasmonic (slow) wave propagating only at frequencies below ω_{SPP} , and it does not experience a cutoff. The TM_0 wave slows down (phase velocity decreases), which is accompanied by the reduction of the group velocity as the frequency is enhanced or the gap thickness is reduced. Here, we should put forward the difference between the TEM of a PEC TL, which is neither a fast nor a slow wave, and the TM_0 plasmonic mode, which is a slow wave leading to reduced

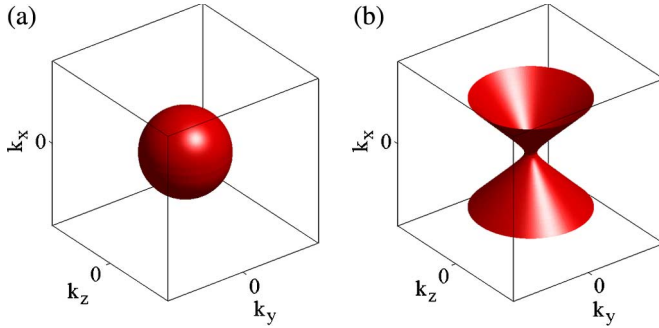


Fig. 4. Reduced diffraction origin for slow waves illustrated in modal k -vector space. (a) For transparent material, the k -vector components are bounded on a sphere translated to diffraction-limited modal size in the spatial space. (b) For SPP (at all media), the k -space is a hyperboloid; thus, k -components are increased simultaneously indefinitely, and hence, the spatial modal size is reduced indefinitely.

diffraction and serving as the main avenue for nanoplasmonic circuitry, as will be discussed later on.

Another issue of interest is the asymmetric plasmonic gap, i.e., metal clad layers are made of different metals [42]. In contrary to a regular dielectric slab waveguide, which exhibits a cutoff even for its zero-order mode, here, TM_0 does not exhibit a cutoff (a plasmonic mode cannot exhibit a cutoff), and its dispersion relation is in between those of the two corresponding single surface plasmons.

Two final points are related to power flow and energy storage by this mode. The power flow of the plasmonic (TM_0) mode is dissected to forward propagation in the dielectric and backward propagation in the metal, which naively may question the integrity of the mode or its usefulness for describing source-mode coupling. This extreme discontinuity of the pointing vector (discontinuity that exists for any TM mode of a dielectric waveguide) on the interface is compensated by a power coupling source at the interface, which is exactly the same surface plasma supporting the TM field discontinuity. Another point of caution is the calculation of stored energy in the metal part, which is important, e.g., for the evaluation of cavity quality or for energy velocity calculations, we should definitely use the following dispersive medium formula: $We = \partial_\omega(\epsilon\omega)|E|^2$.

2) Plasmonic Gap—A Subspace With Reduced Diffraction: We may consider the dielectric material of the gap structure as a subspace with reduced diffraction, which is essential for stepping down into the nanoregime. To better comprehend this fundamental effect, we observe the modal momentum space, which is similar to the discussion by Takahara *et al.* [43].

A dielectric optical cavity cladded by dielectric materials must conform with the k -vector equality $k_z^2 + k_y^2 + k_x^2 = k_0^2\epsilon$, where k_0 is the vacuum wave vector and ϵ is the dielectric constant of the layer. For a regular lossless dielectric configuration, all the elements of this momentum relation are positive within the waveguide core (or cavity core); thus, the propagation wave vector is bounded by a sphere of radius $(k_0\epsilon)^{1/2}$, as illustrated in Fig. 4(a). The classical uncertainty imposes a minimal spatial modal volume of $(\lambda/2)^3$. Replacing the vertical clad layers by metal allows for a plasmon solution, which has a unique feature compared to the aforementioned dielectric case, i.e., an imaginary transverse wave vector in all layers (including the

waveguide or cavity core). The k -vector components relation is modified subsequently to $k_z^2 + k_y^2 - |k_x|^2 = k_0^2\epsilon$. The dielectric constant ϵ is either positive or negative in the dielectric or metal layers, respectively (x is the coordinate normal to metal interfaces). The resulting hyperboloid surface, which is illustrated in Fig. 4(b), has no bound for the vertical wave vector, and moreover, the in-plane k -vector is enhanced by increasing the vertical one. This is in contrary to the characteristics of regular dielectric structures, where by reducing the size in one dimension, the modal size is enhanced in the others. Therefore, there is no apparent fundamental limitation to a minimal modal volume for both normal to the metal layers and in the in-plane directions. Although calculations show that the mode size may shrink to zero for vanishing interface spacing, we restrict the statement to “almost indefinite confinement” since the macroscopic Maxwell equations may fail at a few nanometers scale.

The previous discussion may be interpreted as follows: as the gap width is reduced, the vertical momentum of light inside a plasmonic gap is enhanced. The “slow” nature of this mode leads to a corresponding in-plane momentum enhancement, which is equivalent to the reduction of diffraction. This unique characteristic emphasizes that in order to obtain cavities of subdiffraction modal size in all 3-D, the metal interfaces are required only in 1-D. Inside the reduced diffraction subspace (in between two metal plates), scaled down optical devices (waveguides, cavities, etc.) may support nanoscale modes, which sketches a plausible designing method for optical nanocircuitry.

3) Modeling Losses: Losses, which are intrinsic to the metal-cladded gap structure at optical frequencies, can be added to the model either phenomenologically [11], [12] or by applying a Drude model with loss terms [44] or eventually by incorporation of interpolated experimental information [39], [44], [45]. The structural dispersion relation term (1) is not modified, but complex dielectric constants are used [38]. Few papers looked at the impact of loss on the Fano modes of the real permittivity [11], [12], [44]. The impacts of the loss, in addition to the obvious attenuated propagation of the modes, are the collapse of the plasmon band gap, which is penetrated by Zenneck modes to generate a branch with negative group velocity (gray line in Fig. 2), the propagation of real power into the metal cladding, and the tilt of the amplitude wavefront to compensate for different losses in the core and cladding.

Experimental verification of modal losses [46] of plasmonic gap (Au/SiO₂/Au) was in a good agreement with the calculations based on Drude model.

Some general remarks related to loss in gap waveguide are given. In the red-near-IR wavelength regime, the losses are small enough, such that their main impact is an attenuated propagation [Fig. 3(b)]. The discrete modal spectrum is preserved, with β values pushed slightly from the real axis into the fourth quadrant of Fig. 1. However, at the regime close to plasma frequency, the metal loss dramatically alters the modal characteristics. At a recent paper, Dionne *et al.* considered the implications of the discrepancy of the Drude model from the measured metal permittivity of metals [39], [45]. They reaffirmed that the Drude model (for a complex permittivity)

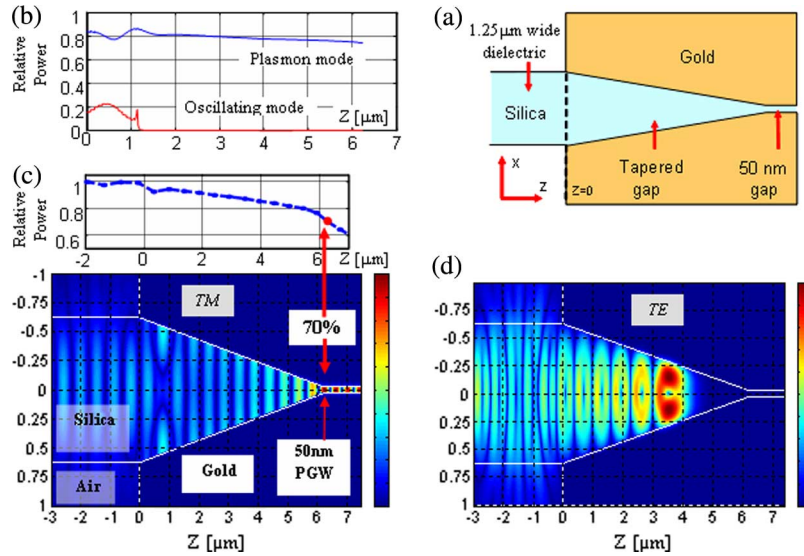


Fig. 5. Plasmonic gap taper (from [15]). (a) Schematics: a 1.25- μm silica slab coupled to 50-nm plasmonic gap via tapered gap. (b) Transfer matrix analysis prediction for the transmitted power versus the propagation distance along the taper. (c) Two-dimensional FDTD simulation result of the pointing vector versus propagation along the tapered plasmon gap waveguide coupler: TM excitation with $\sim 70\%$ transmission (similar to calculations), TE excitation (no plasmon mode exists), oscillating mode is cut off and back reflected.

is valid for the near IR [39], as compared to experimental results [38]. There is no pure distinction between “allowed” and “forbidden” energy bands in the dispersion curve but, rather, solutions with finite propagation length throughout the spectrum. The empirical permittivity values were incorporated into the known dispersion relations, and the complex eigenmodes were solved by converging algorithm based on Nedler–Mead minimization routine in complex wave-vector space.

Since the short propagation length of plasmonic modes is a fundamental limitation, the introduction of gain was discussed either in the broader scope of plasmonic modes [47] or for plasmonic gaps describing the required gain [48]. Unfortunately, the gain factors of known usable media are still not enough to compensate for the metallic loss in nanoscale devices.

B. Modeling Gap Waveguide-Based Devices

For modeling devices based on plasmonic gap, photonic integrated circuit modeling tools as well as methodologies employed in RF circuitry are employed, with some modifications. Some of the most prominent tools include mode-matching techniques and finite-difference time domain (FDTD), which is the tool of choice in the domain of nanophotonics. The subsequent sections exemplify the use of such methods for specific device modeling.

1) *Couplers and Tapers*: In 2005, we reported the surprisingly high-efficiency light coupling into plasmonic gap waveguide, with tapered couplers that can be (and better be) nonadiabatic [49], [50]. Coupling efficiency of $\sim 80\%$ was obtained even when input/output waveguide dimension ratio was 20 and even though the “diffraction limit” point was crossed in the taper toward the nanoscale. The closed-form analysis employed a mode-matching method, i.e., the transfer matrix formalism, to resolve the transmission and reflection of plasmonic gap taper. The tapered coupler was segmented, and mode boundary conditions between segments were applied.

Some assumptions must be emphasized here, i.e., the coupling of TE and TM modes is generally negligible, and only modes of TM family were considered. The number of modes to be traced at each segment is a differentiating factor from a regular dielectric taper; although all the modes here are discrete (see the previous section), many evanescent modes must be considered, since the closure of the system launches the power of these modes, propagating on the interface between the segments, back to the waveguide core. The intrinsic metal loss causes the modal family to be biorthogonal (rather than power orthogonal), hence more coupling coefficients should be calculated and not assumed to be zero. As commented on in [50], this fact stabilizes the numerical procedure. We should point out that adiabaticity is not the optimal solution for plasmonic tapers due to the dominance of the propagation loss and the absence of other forward propagation modes to which to be coupled. Thus, the very short nonadiabatic plasmonic coupler is the optimal solution, as was validated by a 2-D FDTD simulation (Fig. 5).

An analysis of an adiabatic plasmonic taper was reported using the geometrical optics approximation (GOA) [51]. When validated by 2-D FDTD method, discrepancies appear for very small taper angles, which were attributed by the authors to the accumulation of numerical errors in the FDTD method. On the other hand for short tapers, the GOA adiabatic assumption is invalid.

The similarity of the gap waveguides to parallel plate microwave TL can be exploited by borrowing TL design tools. This idea was practiced in the design and simulation of an ultrashort abrupt coupler between two gap plasmon waveguides, using the optimized $\lambda/4$ transformer [41]. The TM wave impedance Z_{TM} , which is determined as the ratio between the transverse parts of the electric and magnetic fields, was calculated, and together with the additional reactance due to the discontinuity, a nanometric long matching segment was designed to yield power transmission efficiency of $\sim 85\%$, as

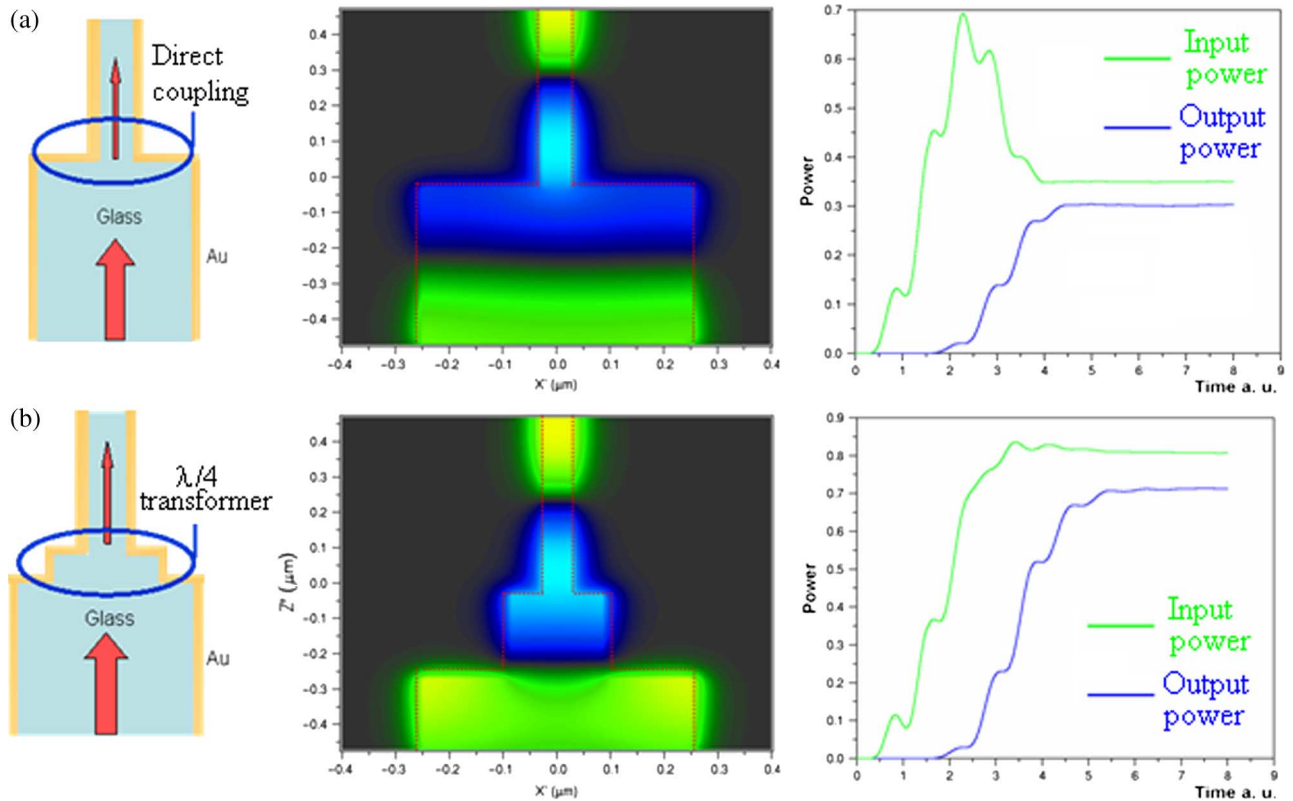


Fig. 6. Plasmonic gap couplers (from [41]). (a) Direct coupling and (b) via $\lambda/4$ coupler; coupler schematics, major magnetic field distribution, and modal power. Extracted from 2-D full-vectorial FDTD simulation with excitation at $\lambda = 1.55 \mu\text{m}$.

validated by FDTD (Fig. 6). A point of interest is the highly efficient direct coupling (with no matching segment), which exceeds significantly the propagating modes overlap. This can be interpreted by a similar mechanism generating the enhanced harvesting in the hole array scenario [37]. Here, the metal walls of the input waveguide serve as reflectors to reproduce multiple images (array) of the output waveguide.

An abrupt coupler was designed by optimization methods and analyzed with 2-D finite-difference frequency domain (FDFD) [52] between a wide dielectric slab and a thin vacuum-filled plasmonic gap. Both waveguides, comprising the coupler, were modified in the vicinity of the interface with optimized segments to improve impedance matching. The 2-D FDFD method is advantageous for stationary [continuous wave (CW)] solutions and for employment of detailed dispersion characteristics, e.g., from experimental data. In addition, they employed a multigrid with a very fine grid resolution of $\sim 1 \text{ nm}$ at the metal–dielectric interfaces. This nonuniform orthogonal grid, which tackles properly the high-contrast metal–dielectric interfaces but does not substantially increase the overall computational complexity, has an undisputable merit particularly for plasmonics.

2) Bending and Junctions: Bended plasmonic gap and T-junction were analyzed with FDFD and compared with the analytical results of PEC-cladded waveguide. The discrepancy between transmission of bends in PEC and real metal gap waveguide is apparent particularly as the wavelength is reduced [53]. The lower cutoff of plasmonic gap compared to the parallel PEC plate TL is due to the smaller wavelength of the

slow plasmonic wave. Incorporating the “effective width effect” into the aforementioned comparison would compensate for the discrepancy. The T-junction results are interpreted by impedance calculations. The T splitter is equivalent to a junction of three TLs with the same characteristic impedance Z_0 . The load connected to the input TL at the junction consists of the series combination of the two output TLs. Thus, the equivalent load impedance is $Z_L = 2Z_0$, and the reflection coefficient is $R = ((Z_L - Z_0)/(Z_L + Z_0))^2 = 1/9$. Because of the symmetry of the structure, the transmitted optical power is equally distributed between the two output waveguide branches, so that the transmission coefficient is $T = 4/9$, as verified by FDTD simulations at long wavelength, where the metal is PEC-like.

The analysis of X-junctions is reported in [54]. The difficulty in using the complete coupling scheme in subwavelength junctions is that due to the closure of the system many high-order evanescent modes play a role and should be incorporated. The modeling in that reference was based on first-order physical reasoning, FDTD simulations, and closed-form analysis with some simplifications. The 2-D FDTD simulations [54] predict a “memory-less splitting: equal power four-port outputs” when light is inserted to a single arm for plasmonic gap thickness $d \ll \lambda$ [Fig. 7(a)]. For wider gap sizes ($\lambda/2 < d < \lambda$), more complex dynamics evolve, including mode beating dynamics. Applying impedance calculations for the X-junction, $Z_L = 3Z_0$, $R = 1/4$, and symmetry results with $1/4$ power in each arm. Therefore, four equal outputs are predicted, which are validated by the simulation for subwavelength gap sizes. The

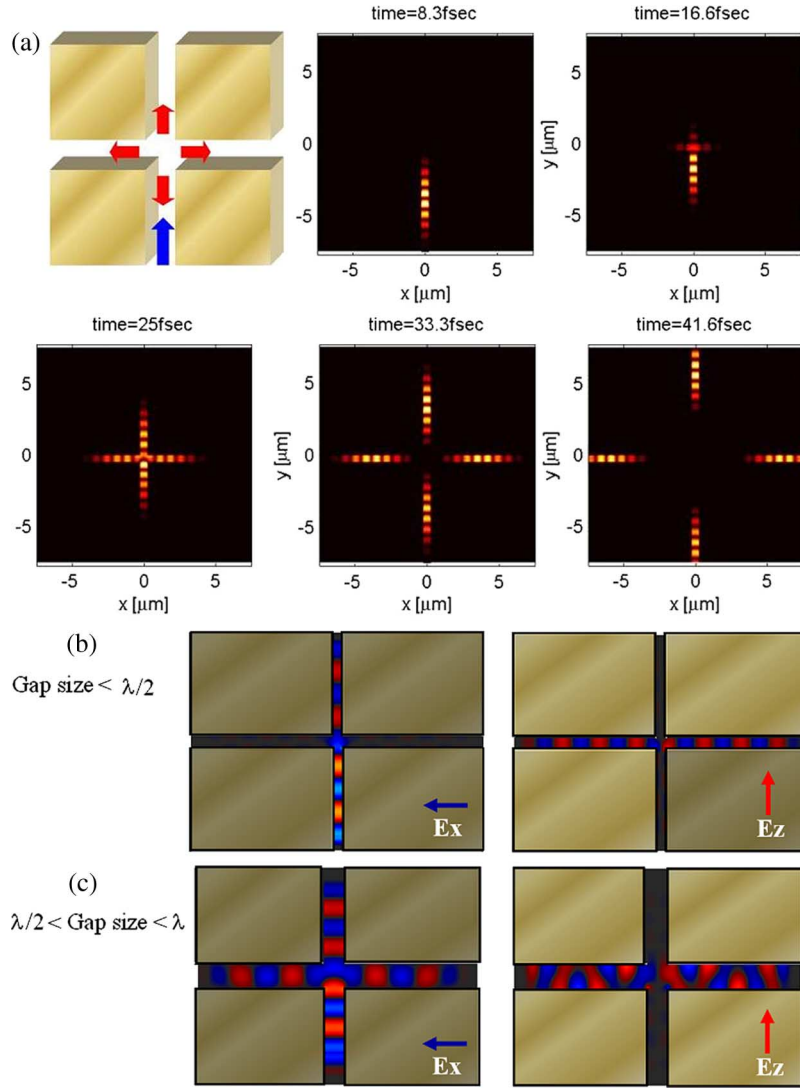


Fig. 7. X-junction. (a) Junction and excitation schematics and perfect four-way splitting example (subwavelength gaps). Polarization split view of CW propagation in X-junction for (b) gap size smaller than $\lambda/2$ and (c) gap size between $\lambda/2$ and λ . FDTD simulation results are both from [54].

impedance analysis employed PEC-like metal, which is reasonable for subwavelength analysis at the near-IR wavelength. When the gap thickness is increased, additional propagating modes are involved. The physical reasoning interprets the input field at the subwavelength junction as a broad azimuthal spectrum source. In the simulations, it appears that a cylindrical wave that is polarized azimuthally enters the junction. Since the basic mode is polarized normal to the gap walls (metal interfaces), the azimuthal polarization perfectly couples to plasmonic TM_0 arm modes. TM_0 is the only propagating mode for $d < \lambda/2$, and the dynamics is simple [Fig. 7(b)]. For thicker gap ($\lambda/2 < d < \lambda$) in the forward going arm, only TM_0 is launched due to the symmetrical excitation, whereas in the side arms TM_0 and TM_1 combination is excited, exhibiting mode beating [Fig. 7(c)].

3) *Coupled Multilayer Gap Plasmon Devices*: If the metal clad thickness is below 100 nm (for practical parameters), the plasmon fields in the gap can be coupled to a neighboring structure, enabling the design of multilayer gap waveguides. The modes of five-layered plasmonic structures were solved by

applying a transfer matrix method, and modal extraction was performed using the reflection pole method [55].

In [56], formalism was derived for extracting recursively the modes of a multilayered structure based on constituting waveguide. This was applied to plasmonic multilayered structures and verified for the five-layer case with direct calculation [57].

III. PLASMONIC COMPLEMENTARY 2-D WAVEGUIDE STRUCTURES

Practical waveguides for plasmonic circuitry should confine light in two dimensions (Fig. 8). In Fig. 8(a) and (b), the 2-D waveguide is formed by a lateral modification of the dielectric internal space of the gap plasmon waveguides, whereas Fig. 8(c) shows an analog of RF waveguide, which is primarily a $\lambda/2$ limited device. All other devices in Fig. 8 are open structures, thus supporting radiation as well as leaky modes (in contrary to the 1-D gap waveguide). This is also critical to the modeling, since proper boundary conditions [e.g., perfectly

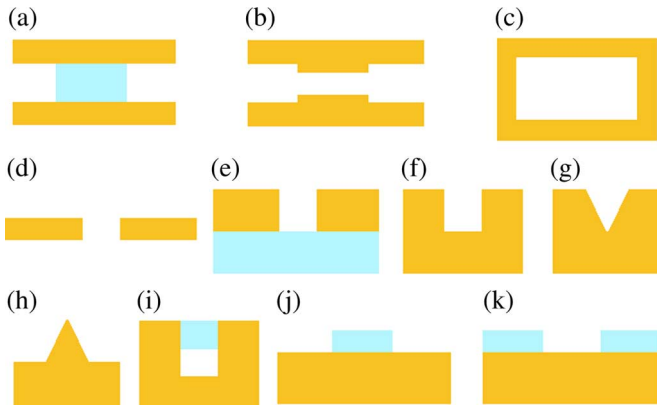


Fig. 8. Plasmonic waveguide structures. (a) Slab within plasmonic gap. (b) Variable size plasmonic gap. (c) Rectangular channel in metal. (d) Slot line. (e) Trench. (f) Rectangular channel. (g) V-groove channel. (h) Metal wedge. (i) Partially loaded channel. (j) and (k) Slab and void layers on metal.

matched layer (PML)] should be employed to capture these modes. In addition, most of these structures belong to class II waveguides, as defined by Oliner and Peng [58] (similar to ridge waveguides), where except for the zero-order mode, only quasi-modes can be guided due to the coupling between TE-like and TM-like modes on the interfaces. In Fig. 8(d) and (e), the slot and trench waveguides can also be considered as TLs (two not simply connected metal layers), whereas all other configurations are based on modified single metal surfaces.

A. Waveguides Within a Plasmonic Gap

Exploiting the reduced diffraction subspace that exists in between the metal layers of the gap structure, one can implement plasmonic circuitry by employing in-plane dielectric boundaries. The notion of reduced diffraction that is vertical gap width-dependent fits well the concept of the EI method, which is a very important modeling engine for plasmonic structures. The EI analysis, which is easily implemented and interpreted, was found valid for many configurations of 2-D plasmonic void waveguides, as will be discussed in the subsequent section.

The effective index is the propagation constant divided by free-space wavenumber. For slow waves, it is higher than the actual index of the dielectric (filling the plasmonic gap). Therefore, the effective indexes as well as the in-plane core/clad effective indexes ratio are higher than the respective material values, such that regular dielectric structures within a gap can support subdiffraction modes.

A dielectric stripe within a plasmonic gap [Fig. 8(a)] was analyzed with FDTD [59] simulations, and the results were compared to the EI calculations. Although the EI method is not a completely rigorous tool and may fail, particularly when the refractive index difference is large, it was found that the EI predictions match well the FDTD results for the embedded waveguide. Here, the EI method is applied first to the (fast) vertical dimension (normal to the metal interfaces), and subsequently, the calculated effective indexes of the plasmonic (TM_0) modes were assigned as the in-plane index profile.

The effective index of the gap structure also depends on the permittivity of the metal plates, hence using an assembly with different lateral metals (termed metal heterowaveguide)

can serve to confine the mode in the in-plane dimension [60], as was verified with FDTD simulation.

In [61], the waveguide cross section is a rectangular air channel in metal, with a reduced metal gap in its center where the wave is actually guided [Fig. 8(b)]. The structure may be considered as composed of three plasmonic gaps, with the central one having a reduced gap size and, thus, higher EI. The EI incentive is verified by a volume integral equation discretized by pulse-function and point-matching collocation method. The resultant linear equations were resolved by a generalized conjugate residual iteration combined with fast Fourier transform. Using this guiding concept, a waveguide splitter was studied as well. The modal propagation constant (according to standing waves periods) matches reasonably the calculated effective indexes, but the EI method was quantitatively successful only for relatively small gap thickness difference. This theme was continued in [62] for N -arms multiplexer. The structure size was $0.88\lambda \times 0.86\lambda \times 0.51\lambda$, and it was discretized uniformly with 0.008λ resolution. The multiplexer performance was substantially sensitive to structural modifications, necessitating highly accurate simulations. This example elucidates the difficulty of simulating plasmonic devices, due to nanometric grid requirements.

Finally, the fully inclosed rectangular air channel in metal [Fig. 8(c)] was examined by EI analysis and FDTD simulations, and only slight variations were exhibited between the two [63]. The simulation results were also compared to PEC metal, which gives distinctive cutoff values. For PEC, the cutoff is exhibited for a gap width of $\lambda/2$. For the real (Drude) metal, the cutoff wavelength was enhanced by 41%. The FDTD calculations showed that the material loss did not influence the cutoff wavelength and was negligible for wavelengths just a few nanometers above the cutoff wavelength.

B. Modeling Plasmonic Slots and Trenches

We first dwell with symmetrical open system, i.e., a waveguide embedded in a homogenous dielectric (same substrate and superstrate). This applies only to the slot and trench waveguides [Fig. 8(d) and (e)], due to the built-in asymmetry of all the channel waveguides. Symmetry is crucial, since even slight asymmetry may result in a cutoff of nanosized modes. The slot configuration is supported by a very thin metal (order of skin depth), and as such, the dominant mode will be the TM modes of the metal layers coupled via the slot. However, as the metal thickness is increased, the vertical sidewalls of the trench can support their own plasmonic mode, which is the TE mode in our scheme (see the inset of Fig. 9).

For highly symmetrical structure, the EI method predicts the existence of bound modes in a slot (e.g., 20-nm metal thickness) or trench (e.g., 400-nm metal thickness), for any wavelength or width. Full-vectorial H-field finite-difference (FVHFD) simulations of gold trenches were verified by measurements [64]. H-field is the better choice for mode solvers or propagation schemes of plasmonic structures due to the large discontinuity of the E-field on the interfaces. Both the simulation and experiments resulted in a hybrid mode with a "TE-like" component confined in the trench. However, for

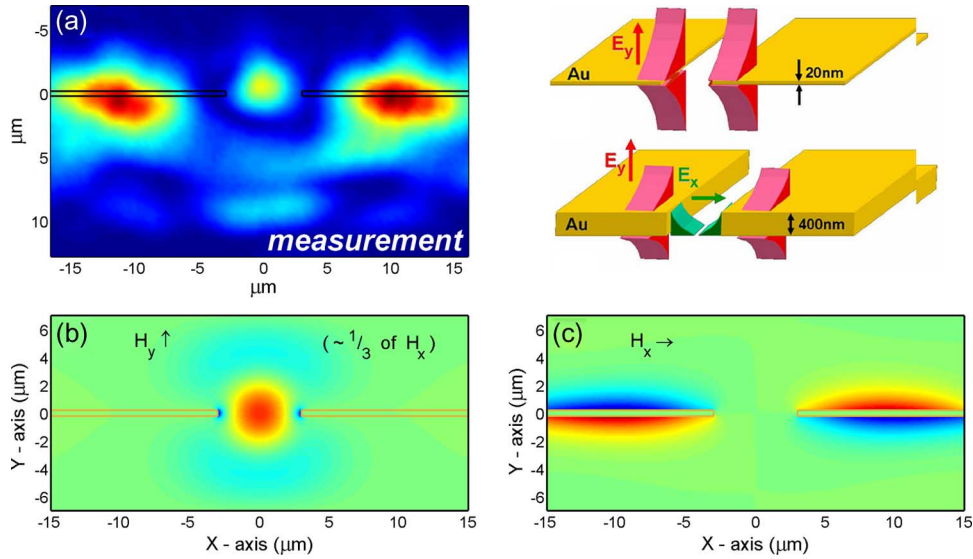


Fig. 9. Modal pattern of a 10- μm -wide trench engraved in a 400-nm-thick gold layer, embedded in a dielectric host ($n = 1.5$), with the TE (E_x field) excited at $\lambda = 1.55 \mu\text{m}$. The gold layer borders are graphically illustrated. (a) Experimental imaging of optical power at the output facet in comparison to FVHFD-calculated guided mode (second mode). (b) E_x/H_y electromagnetic field component peak value is 3.5 times higher than the (c) E_y/H_x electromagnetic field components. Inset: Symmetrical SPP waveguide structures studied: (Upper) slot and (lower) trench (from [64]).

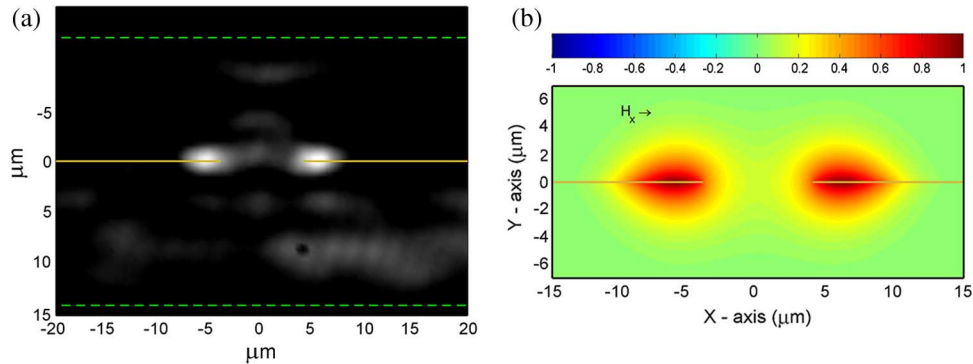


Fig. 10. (a) Modal pattern measurement of an 8- μm -wide slot made in a 20-nm-thin gold slab, with TM excitation at $\lambda = 1.55 \mu\text{m}$. (b) FVHFD calculation with TM excitation resulting to SPP-assisted slot mode, as $n_{\text{eff}} = 1.502534 - j \cdot 0.0001544$. The location of the metal stripe is graphically drawn as a golden solid line, as BenzoCycloButene (BCB) cladding borders are drawn as green dashed lines (from [65]).

a symmetrical slot configuration, neither the simulation nor the experiments gave the confined mode predicted by the EI method, only the surface-like TM mode [65] (Fig. 10). This may be due to either (or both) failure of the EI method at such low confinement scenario or (and) the problematic excitation of this mode. The two first modes of a slot in a thin metal film waveguide were further explored with compact 2-D FDTD and FDTD and experimentally validated [66]. The lowest mode does not exhibit a cutoff, as the metal layer is thinned. For a thick metal layer, the effective index for both modes is similar to that of a plasmonic gap.

Nanometric size asymmetrical slot waveguide (silica–air) in a 50-nm-thick Ag film and with aspect ratio of 1 (50-nm gap) was examined in [60] with H-field full-vectorial FDFD mode solver. Since the slot dimensions are much smaller than the wavelength in the frequency range of interest, the fundamental bound mode is quasi-TEM with dominant field components E_x and H_y , and this waveguide does not support any higher order bound modes. Since the fundamental mode is quasi-

TEM, it can be efficiently excited by linearly polarized light. The dispersion curve is showing slow modes as expected. It should be emphasized that a PEC slot line does not support a bound mode (although the leaky mode may have small radiation loss). The slow wave characteristic of the plasmon is what enhances its effective index above the surrounding material to produce a bound mode. The modal size remains small even at low frequencies where the dispersion relation approaches the silica light line, which is a completely distinctive characteristic compared to that of a dielectric waveguide mode approaching a cutoff. This may explain the extended usefulness of the EI method for plasmonic slot trench, even close to cutoff, since the mode retains its high confinement.

Similar slot-line structure was analyzed with the FDTD method [67], as well as its arrays and bending. EI notion was utilized to explain the confinement. A more elaborated EI analysis of such structure was presented with comparison to 2-D FDTD results [68]. In this paper, the mode in the trench is calculated (using complex permittivity), and the EI is used to

solve a three-layer TE mode. The EI mode calculations match very well the values obtained by the FDTD simulations (for the mode supported by the trench metal interfaces), and the fit was better as the metal film thickness was increased.

It should be emphasized that the asymmetrical slot-trench configurations are nanodevices by nature. Only nanometric wide slot trench can support a confined mode in an asymmetrical environment. Again, EI interpretation to the latter is obvious, i.e., one has to narrow the slot to the nanoregime in order to generate slower plasmon, which has EI larger than the actual index of the higher index substrate. Unfortunately, the thickness/width aspect ratio of the slot trench should also be raised substantially, such that implementation may become challenging.

C. Modeling of Plasmons on Deformed Single Surface (Channel and Edge Waveguides)

A unique family of waveguides supporting 2-D bound plasmonic modes is the deformed single metallic surface. While similar structures using PEC may guide leaky waves, here bound modes on corners, edges, and channels can propagate. The channel plasmon-polariton (CPP) is the distinguished member of this family, and recently, waveguides and devices based on CPP were fabricated and measured [69], [70].

Rectangular and V-groove CPPs were analyzed with EI method [68]. The model is applied with the fast axis parallel to the metal layer. The V-groove was subsectioned to variable thickness “gap” waveguides. The final calculation was for the TE mode of a multilayer structure, i.e., air–EI layers–metal. Since reduction of the gap size results to EI enhancement, the CPP mode confinement is better in narrower grooves (at the expense of larger damping). However, generally, the modes propagating on small deformations are highly hybrid, and the EI method is not readily applicable; therefore, other modeling methods should be employed. Similar modes also appear in highly asymmetrical slot configuration (Si–air) as corner modes (calculated by full-vectorial H-field finite element method (FVHFEM) in [71]).

An analysis of guided modes on a deformed metal interface was performed, based on the modified moments method [72]. Since it is based on Green functions and using discrete point matching at finite resolution around the metal edge, it may be nonoptimized for abrupt surface changes; however, it is a fundamental method that can be adapted to the plasmonic scenarios. It is based on an ordinary method of moments but then uses some specific assumptions for single interface guidance. The model is applied to CPP modes, assuming real permittivity, even though it is possible to incorporate a complex one into the model.

A similar method, such as multiple multipole method (MMP), was applied for CPP and verified by FDTD simulations, where the metal dispersion was interpolated by measured values [73]. The dispersion curves of MMP (calculated with 10-nm resolution) and FDTD (5-nm resolution) are very similar.

Several FDTD simulations of CPP were reported [70], [74], [75]. In [70], a good match with EI results as well with exper-

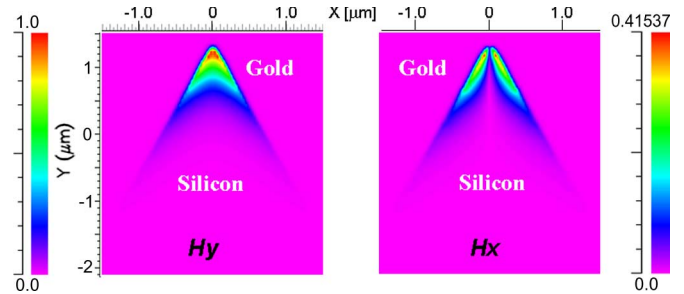


Fig. 11. FVHFEM calculations of 55° silicon-filled V-groove in gold. The two transverse H-fields are given (from [76]).

iments is given. Results of FVHFEM calculations are shown in Fig. 11, emphasizing the hybrid mode characteristics (the two polarizations have similar magnitudes) [76]. In [77], a half-loaded rectangular CPP [Fig. 8(i)] mode is studied by a finite-difference mode solver, and its coupling scheme is studied with FDTD and compared to an experiment. The measured loss was substantially higher (~ 0.2 dB/ μ m) than the predicted one.

Similar analysis was also performed to the complementary wedge structure. The wedge plasmon-polaritons (WPP) were studied by compact 2-D FDTD, FDTD, and experimentally [78]. An excitation artifact obtained in the FDTD algorithm resulted in a snakelike pattern due to the interference of the wedge mode and the surface plasmons on the sides of the wedge. To overcome this artifact, an entrance aperture was realized to reduce the excitation of sidewall surface modes (both in simulation and in the actual experiment). This, for example, is a disadvantage of the compact 2-D FDTD; however, it is faster and, as argued in [78], results in more accurate modal distributions. This example is discussed here to emphasize the importance of a proper excitation of these types of discontinuity waveguides, both for modeling and measurements.

Retardation-less (“electrostatic modes”) assumption obviously simplifies the analysis of these structures; the transverse wavenumber is assumed to be the same in both media adjacent to the interface, hence the field along the interface is solvable analytically [79]–[83]. Including the retardation effects, WPP modes that are much smaller than the wavelength are calculated using a full-fledged mode expansion analysis [84]. Unique field distributions and dispersion curves are observed. The analysis (necessarily) involves not commonly used optimal basis functions set with solutions that are a limited bandwidth series of the basis functions. We found that the retardation-less analysis coincides asymptotically for high propagation constants and exhibited sub- $\lambda/2$ modal sizes (Fig. 12).

Finally, in [85], a different type of 2-D plasmonic waveguide was suggested and analyzed [Fig. 8(j) and (k)]. The vertical confinement is by a single surface plasmon, and the single surface is loaded by a different dielectric (laterally). In segments where the dielectric layer is loading the metal surface, the vertical mode is modified, and so is its effective index. The EI method is found to be within 1% accuracy for the fundamental modes in comparison to FDFD mode solver for few frequencies, as demonstrated for several structures.

To conclude this section, the modeling of the edge-channel configurations (being very unique to slow modes) can be

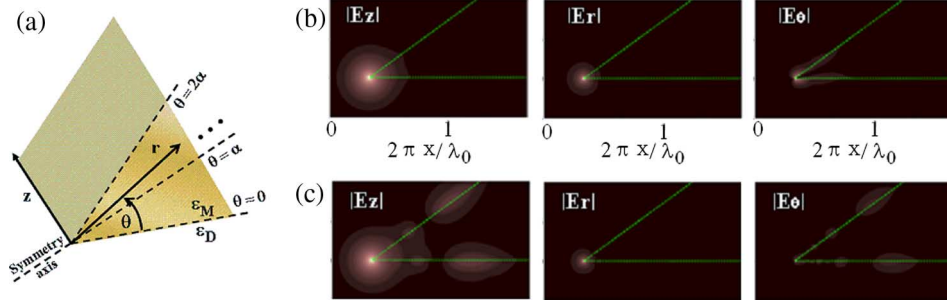


Fig. 12. Hybrid polarization nanosized modes of metal wedge. (a) Schematics. (b) and (c) Modal full-fledged analysis and E-field component distributions (from [84]).

categorized in to finite-difference propagators, simplified solution of nonretarded schemes, and full-fledged solutions. Finite-difference propagators may miss the modes, which are very small, are usually highly lossy and require special excitation, and may yield mainly single surface slow modes close to the light line or fast modes. Retardation-free solutions are only asymptotic approximations, whereas full-fledged solutions are very problem dependent.

IV. CAVITIES WITHIN PLASMONIC COMPLEMENTARY STRUCTURES

An optical cavity realized in a plasmonic gap may turn out to be the better way for achieving much below $1\lambda^3$ dimensions supporting nanosized modes in all three dimensions with a reasonable quality factor.

A Fabry-Pérot cavity inside a plasmonic gap that is $3\ \mu\text{m}$ long in 1-D but nanosized in the other two (55–483 nm wide and 3.3–14 nm thick) was analyzed by employing the 2-D boundary element method, as well as fabricated and actually measured [86], [87]. Partial agreement was obtained by comparing the theoretical and experimental results (not all the transmission dips were reproduced by the calculation). Experimental results validated the analytical dispersion curves of the gap waveguides. These results are highly encouraging as they indicate both the validity of macroscopic (continuous) electromagnetics with no spatial dispersion effects down to a gap thickness of 3 nm (at least as far-field response is discussed) and the quantitative guidance model for gap plasmons (the observed short wavelengths validates the predicted “reduced diffraction”). Theoretical claim sets a gap thickness of 1.5 nm as the limitation for continuous electrodynamics and the local Drude model [51].

A complete 3-D dielectric cavity within the plasmonic gap was modeled, exploiting the reduced diffraction concept [88], [89]. This structure is beneficial both for reducing the vertical leakage (no vertical radiation modes as discussed) and for allowing unlimited shrinkage of the modal volume. The dielectric cavity was designed as a cavity in photonic bandgap structure [89] or as a simple cylinder [88]. The modeling results were validated by the (FDTD) numerical solutions of Maxwell equations. In this configuration, each calculation box dimension is smaller than half of the wavelength, and a PML is used for boundaries.

The EI method that is conventionally used to extract the propagation constant and modal fields of a waveguide structure was employed here very successfully to calculate the eigenfrequencies and modal fields of a 3-D cavity. The fast direction of the EI method was taken vertically to the layers (the shortest dimension of the structure). The propagation constant of the TM_0 gap mode was resolved from the dispersion relations, both inside and outside the dielectric cylinder. The modal effective index is assigned, generating a 2-D in-plane equivalent structure of a dielectric circular cavity. The boundary conditions for each (m) azimuthal order yield a set of discrete radial solutions (indexed by l), each having a distinct modal frequency.

The definition of modal volume is an involved issue, particularly when metal is involved. While most of the cavity-related literature is using the effective mode volume from the Purcell effect calculations [90], we believe that this effective mode volume (while being important for exhibiting the Purcell effect) is mostly the spatial intensity enhancement factor at the point of maximum intensity rather than the “actual mode volume.” Furthermore, this measure has nothing to do with diffraction effects, which are related to the “uncertainty” of the mode distribution, such as the intensity distribution variance. Since a major fundamental interest is the relation between plasmonic cavities and diffraction, we characterized our structure by a mode “uncertainty” volume $V = D_{\text{eff}}^3 = \pi R_{\text{eff}}^2 h_{\text{eff}}$, where R_{eff} and h_{eff} are the variance of the intensity distribution along the radius and height, respectively. In order to facilitate the comparison with other reported cavities, the Purcell effective mode volume is provided as well, which always yields a significantly lower value (Fig. 13).

For a specific structure excited by a broad-band pulse (as in the following FDTD simulations), the modal wavelength is specific to the given cylinder radius [Fig. 14(a) and (b)]. A unique feature in the plasmonic-assisted cavity is that higher Q -factors are expected for high-order modes, which is counter-intuitive with the common wisdom of regular dielectric cavities. For regular cavities, higher order in-plane modes have lower vertical k -vector, resulting in enhanced vertical radiation losses. For the “plasmonic” cavity, the metal layers disallow vertical radiation; however, they are a source for material loss. The in-plane radiation loss into the dielectric clad decreases with the order of the mode. Mathematically, it can be traced to the fact that the solution outside the core ($r > a$), which is a Hankel

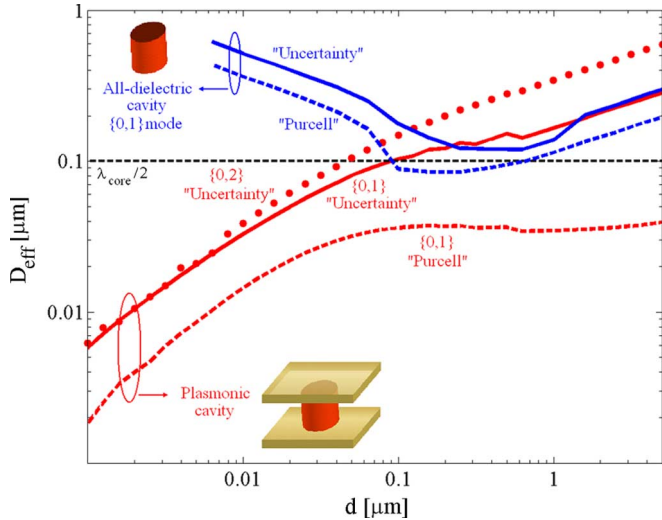


Fig. 13. Nanosized cavity–dielectric cylinder embedded in plasmonic gap. Averaged modal size (calculated with EI method) versus cylinder height at $\lambda_0 = 700$ nm. $n_{\text{Si}} = 3.5$, $n_0 = 1$, $\lambda_{\text{plasma}} = 137$ nm (from [88]).

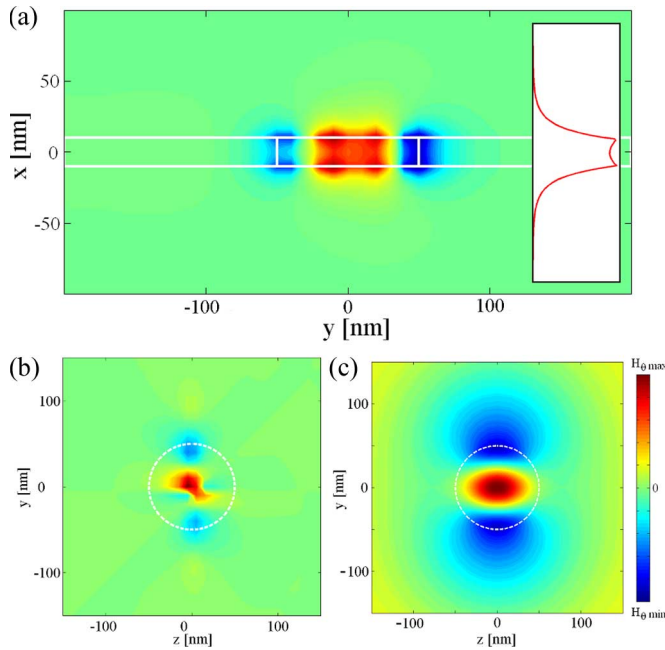


Fig. 14. FDTD simulations. Metal thickness is 100 nm (practically infinite). A short x polarized pulse inside the cavity results to a major spectral peak at ~ 700 nm. H_θ distribution. (a) Vertical plane at $z = 0$ (from the higher resolution CW excitation at 700 nm). Inset: Field profile along x , at $y = 20$ nm. (b) In-plane at $x = 0$ (from the impulse excitation since CW has poorer visualization due to interference with the continuous source). (c) Calculations by the EI method for $\lambda_0 = 700$ nm. Cylinder boundaries in white dashed line (from [88]).

function of the second kind, vanishes rapidly for higher orders. However, larger material losses are typical to higher order modes. This interplay results in an optimized quality factor for modes of intermediate orders.

FDTD, incorporating the complex metal dielectric function of the Drude model, was used to simulate a silicon cylinder with 100-nm diameter in a 20-nm gap between gold plates. The resulting major cavity mode has a spectral peak of ~ 700 nm (examined with broad-band pulse and CW at the major cavity

mode wavelength). The intensity full-width at half-maximum resolved effective modal volume of 36 nm^3 is more than an order of magnitude smaller than the “diffraction limit” and has a Q -factor of 170, which is calculated by the ratio of total stored energy in a volume encompassing the cavity and the total outgoing power from the volume surfaces. The Q -factor can be further enhanced by employing lower loss metals (e.g., silver) or for increased intermetal gap.

The EI analysis for these structure parameters (air gap of 20 nm between gold plates) also predicts that the balance between the vertical metal losses and in-plane radiation losses retains the $\{0, 2\}$ and $\{2, 1\}$ modes, both having similar eigen-frequencies of about 700 nm. Their interference [Fig. 14(c)] matches the mode distribution and spectrum as obtained in the FDTD simulation [Fig. 14(b)], and the expected axial rotation of the pattern is due to the slight difference in the modal propagation constants. The calculated field confinement is slightly smaller compared to the simulation results—the effective modal volume of 41 nm^3 , which may be due to the influence of the imaginary part of the metal dielectric constant—not included in the effective index analysis.

V. KERR NONLINEARITY WITHIN GAP PLASMONIC WAVEGUIDES

The plasmonic gap can be loaded with nonlinear medium, thus combining nanoscale modes, enhanced intensities, and self-guiding mechanism. Incorporating a Kerr nonlinearity as a first case modeling yields the possible evolution of a novel hybrid-vector plasmon–soliton.

The novel soliton was modeled by a modified nonlinear Schrödinger equation (NLSE), encompassing hybrid-vector field characteristics [91]. Assisted by the transverse plasmonic effect, the self-trapping dimension of the plasmon–soliton was substantially compressed (compared with a dielectrically cladded slab case) when the slab width was reduced. The practical limitation of the plasmon–soliton size reduction is determined by the availability of nonlinear media and metal loss. For the extreme reported values of nonlinear index change, we predict a soliton with a cross section of 300×30 nm (average dimension of 100 nm).

From the modeling perspective, the reduced diffraction of the plasmon in a gap is instrumental for a proper transformation of Maxwell equations to the NLSE of the envelope function for ultrasmall solitons. Nevertheless, the enhancement of the nonlinear effect is not proportional to the linear reduced diffraction [Fig. 15(a)].

A general NLSE for transverse TM modes with lateral (in-plane) nonlinear confinement was derived by taking into account the two electric field components. The derivation assumes that the TE/TM modes of the layered structure hold, which is reasonable when the in-plane soliton width Δy is significantly larger than the mode vertical width Δx . A scalar wave equation [aligned parallel to the $E = (E_x, 0, E_z)$ field] could be derived and transformed to a nonlinear Schrödinger equation by employing a paraxial approximation and averaging over x . A unique first-order plasmon–soliton emerges. The same scenario when applied to Kerr medium confined by regular dielectric

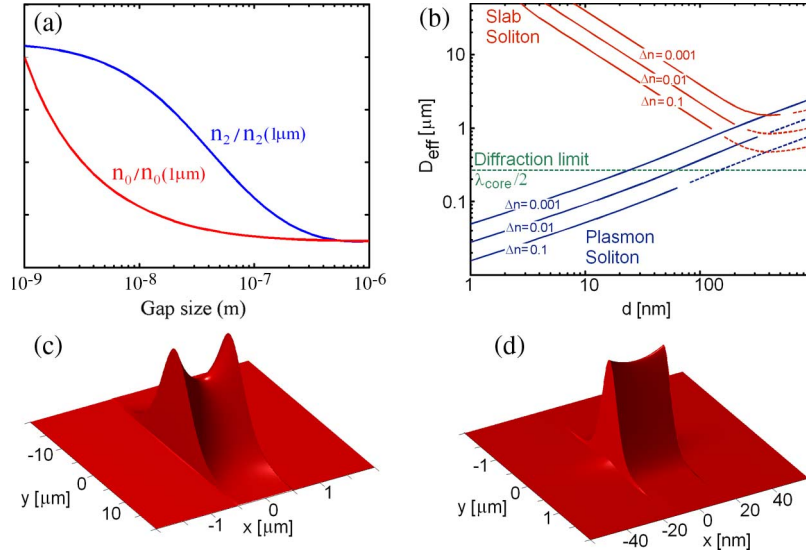


Fig. 15. (a) Normalized (red) linear and (blue) nonlinear effective indexes inside plasmonic gap at $\lambda_0 = 1.5$ μm . (b) Effective modal size D_{eff} versus gap thickness of the nonlinear Kerr slab embedded in (blue) metal and (red) air. $\lambda_0 = 820$ nm, $n_0 = 1.5$. Intensity distributions of plasmon-soliton beam in Kerr medium embedded within silver layers. (c) $\Delta n = 0.005$, $\lambda_0 = 1550$ nm, $d = 1$ μm , $\epsilon_m = -30.2 - i1.6$, $D_{\text{eff}} = 95$ nm (from [91]). (d) $\Delta n = 0.1$, $\lambda_0 = 820$ nm, $d = 30$ nm, $\epsilon_m = -30.2 - i1.6$, $D_{\text{eff}} = 95$ nm (from [91]).

yields effective soliton dimension with a minimum at slab thickness of $\sim \lambda/2$ [see Fig. 15(b)]. The soliton confinement cannot be enhanced further by increasing the intensity, as the nonlinear index change reaches its saturation value.

However, for the nonlinear plasmonic gap, the “plasmonic” effect is shown to overcome this minimum effective soliton width restriction. The unique role of the reduced diffraction of the plasmonic wave is quantified by a factor I_3/I , which weights the nonlinear coefficient n_2 . I_3 is the vertically integrated squared intensity in the core, and I is the total integrated intensity, and thus, the factor I_3/I is the figure of merit for the intensity localization in the nonlinear segment (dielectric core). It turns out that decreasing the plasmonic gap size modifies differently the linear and nonlinear “diffraction” terms, as illustrated in Fig. 15(a). While the linear effective index increases rapidly, as the gap size is reduced, the nonlinear index enhancement saturates.

Solving for a nonlinear Kerr medium that is in between two silver layers yields a closed-form expression for the soliton width. The Kerr media used in the calculations include nonlinear glasses, exhibiting a nonlinear index change of 10^{-3} , as well as materials exhibiting the extreme high index change of 0.1 [effective size: Fig. 15(b); intensity trace: Fig. 15(c) and (d)]. The “plasmonic” signature is evident; in contrast to the minimum of D_{eff} exhibited for dielectric clad, here, the effective size may be reduced with gap thickness, and nanoscale dimensions below the diffraction limit ($D_{\text{eff}} < 100$ nm) are achievable.

The two major physical sources limiting the compression of the plasmon-soliton beam size are the maximal attainable nonlinear index change and the mode attenuation. As the effective wavelength in the plasmonic gap is reduced (shorter free-space wavelength or narrower gap), the mode attenuation becomes larger, setting a practical limit on the plasmonic-assisted reduced diffraction. Yet, the fundamental saturation of the factor I_3/I for reduced gap sizes limits the soliton lateral width

Δy to the diffraction limit dimension. Therefore, attainable plasmon-soliton beams may have a lateral size of about the diffraction limit and a transverse size of a few tens of nanometers.

VI. CONCLUSION

As evident from this paper, the field of plasmonic complementary waveguides is in a formation stage with exciting results. A large variety of plasmonic configurations is offered, taking advantage of the possibility of guiding plasmons on single interface metallic waveguides within a rich ensemble of complementary (void) structures and on nanoscale discontinuities (e.g., edges and corners). The shaped channel waveguide and the edge guiding may serve as a prototype for nanoscale plasmonic elements.

The various analyses and simulation methodologies were adopted from photonics and microwave TLs and were successfully modified to the plasmonic field. Good results were obtained for micrometer size modes and for the mesoscopic submicrometer regime to a few hundred nanometers. However, most of these methods are not trivially implemented in the deep nanoscale regime, and this should be the direction for future modeling.

The EI method, even though it is not a rigorously proven method, provides first-order compatible results, as shown in several comparisons to experiments and other numerical methods. The relative success of the EI method can be attributed to the highly confined nature of the plasmonic mode, which is even close to cutoff.

Finite-difference methods (FDTD, FDFD, etc.) are very common and useful. However, some caution should be exercised when modeling plasmonic waveguides.

- 1) A very high resolution (1 nm) should be applied at the high-contrast metal-dielectric interfaces. Proper interface smoothing should be applied for difference method stability.

- 2) The nanosized plasmonic slow wave is characterized by very small modal cross section, high losses, and complex source mode coupling. Methods of filtering out other modes and designing proper excitation schemes are crucial to track the modes of interest.

ACKNOWLEDGMENT

The authors would like to thank Y. Stav (Satuby), D. Arbel, and P. Ginzburg for contributing a part of the material for this paper.

REFERENCES

- [1] W. L. Barnes, A. Dereux, and T. W. Ebbesen, "Surface plasmon subwavelength optics," *Nature*, vol. 424, no. 6950, pp. 824–830, Aug. 2003.
- [2] E. Ozbay, "Plasmonics: Merging photonics and electronics at nanoscale dimensions," *Science*, vol. 311, no. 5758, pp. 189–193, Jan. 2006.
- [3] S. A. Maier, "Plasmonics: The promise of highly integrated optical devices," *IEEE J. Sel. Topics Quantum Electron.*, vol. 12, no. 6, pp. 1671–1677, Dec. 2006.
- [4] S. A. Maier and H. A. Atwater, "Plasmonics: Localization and guiding of electromagnetic energy in metal/dielectric structures," *J. Appl. Phys.*, vol. 98, no. 1, p. 011 101, Jul. 2005.
- [5] W. L. Barnes, "Surface plasmon–polariton length scales: A route to subwavelength optics," *J. Opt. A, Pure Appl. Opt.*, vol. 8, no. 4, pp. S87–S93, Apr. 2006.
- [6] D. Huang, T. Sze, A. Landin, R. Lytel, and H. L. Davidson, "Optical interconnects: Out of the box forever?" *IEEE J. Sel. Topics Quantum Electron.*, vol. 9, no. 2, pp. 614–623, Mar. 2003.
- [7] J. Homola, S. S. Yee, and G. Gauglitz, "Surface plasmon resonance sensors: Review," *Sens. Actuators B, Chem.*, vol. 54, no. 1, pp. 3–15, Jan. 1999.
- [8] U. Fano, "The theory of anomalous diffraction gratings and of quasi-stationary waves on metallic surfaces (Sommerfeld's waves)," *J. Opt. Soc. Amer.*, vol. 31, no. 3, pp. 213–222, Mar. 1941.
- [9] R. H. Ritchie, "Plasma losses by fast electrons in thin films," *Phys. Rev.*, vol. 106, no. 5, pp. 874–881, Jun. 1957.
- [10] E. N. Economou, "Surface plasmons in thin films," *Phys. Rev.*, vol. 182, no. 2, pp. 539–554, Jun. 1969.
- [11] J. J. Burke, G. I. Stegeman, and T. Tamir, "Surface-polariton-like waves guided by thin, lossy metal films," *Phys. Rev. B, Condens. Matter*, vol. 33, no. 8, pp. 5186–5201, Apr. 1986.
- [12] F. Yang, J. R. Sambles, and G. W. Bradberry, "Long-range surface modes supported by thin films," *Phys. Rev. B, Condens. Matter*, vol. 44, no. 11, pp. 5855–5872, Sep. 1991.
- [13] P. Berini, "Plasmon–polariton waves guided by thin lossy metal films of finite width: Bound modes of symmetric structures," *Phys. Rev. B, Condens. Matter*, vol. 61, no. 15, pp. 10 484–10 503, Apr. 2000.
- [14] J. C. Weeber, Y. Lacroute, and A. Dereux, "Optical near-field distributions of surface plasmon waveguide modes," *Phys. Rev. B, Condens. Matter*, vol. 68, no. 11, p. 115 401, Sep. 2003.
- [15] T. Nikolajsen, K. Leosson, I. Salakhutdinov, and S. I. Bozhevolnyi, "Polymer-based surface-plasmon–polariton stripe waveguides at telecommunication wavelengths," *Appl. Phys. Lett.*, vol. 82, no. 5, pp. 668–670, Feb. 2003.
- [16] J. R. Krenn, B. Lamprecht, H. Ditlbacher, G. Schider, M. Salerno, A. Leitner, and F. R. Aussenegg, "Non-diffraction-limited light transport by gold nanowires," *Europhys. Lett.*, vol. 60, no. 5, pp. 663–669, Dec. 2002.
- [17] R. Charbonneau, P. Berini, E. Berolo, and E. Lisicka-Shrzek, "Experimental observation of plasmon–polariton waves supported by a thin metal film of finite width," *Opt. Lett.*, vol. 25, no. 11, pp. 846–884, Jun. 2000.
- [18] A. Boltasseva, T. Nikolajsen, K. Leosson, K. Kjaer, M. S. Larsen, and S. I. Bozhevolnyi, "Integrated optical components utilizing long-range surface plasmon polaritons," *J. Lightw. Technol.*, vol. 23, no. 1, pp. 413–422, Jan. 2005.
- [19] V. A. Podolskiy, A. K. Sarychev, E. E. Narimanov, and V. M. Shalaev, "Integrated resonant light interaction with plasmonic nanowire systems," *J. Opt. A, Pure Appl. Opt.*, vol. 7, pp. S32–S37, 2005.
- [20] P. Berini, "Plasmon–polariton waves guided by thin lossy metal films of finite width: Bound modes of asymmetric structures," *Phys. Rev. B, Condens. Matter*, vol. 63, no. 12, p. 125 417, Mar. 2001.
- [21] R. Zia, M. D. Selker, and M. L. Brongersma, "Leaky and bound modes of surface plasmon waveguides," *Phys. Rev. B, Condens. Matter*, vol. 71, no. 16, p. 165 431, Apr. 2005.
- [22] C. A. Pfeiffer, E. N. Economou, and K. L. Ngai, "Surface polaritons in a circularly cylindrical interface: Surface plasmons," *Phys. Rev. B, Condens. Matter*, vol. 10, no. 8, pp. 3038–3051, Oct. 1974.
- [23] B. Prade and J. Y. Vinet, "Guided optical waves in fibers with negative dielectric constant," *J. Lightw. Technol.*, vol. 12, no. 1, pp. 6–18, Jan. 1994.
- [24] U. Schröter and A. Dereux, "Surface plasmon polaritons on metal cylinders with dielectric core," *Phys. Rev. B, Condens. Matter*, vol. 64, no. 12, p. 125 420, Sep. 2001.
- [25] S. J. Al-Bader and M. Imtaar, "TM-polarized surface-plasma modes on metal-coated dielectric cylinders," *J. Lightw. Technol.*, vol. 10, no. 7, pp. 865–872, Jul. 1992.
- [26] J.-C. Weeber, J. R. Krenn, A. Dereux, B. Lamprecht, Y. Lacroute, and J. P. Goudonnet, "Near-field observation of surface plasmon polariton propagation on thin metal stripes," *Phys. Rev. B, Condens. Matter*, vol. 64, no. 4, p. 045 411, Jul. 2001.
- [27] J. Kim, J. Kim, and K.-H. Park, "Local excitation of surface plasmon in structured Au films by atomic force anodic oxidation," *J. Vac. Sci. Technol. B, Microelectron. Process. Phenom.*, vol. 22, no. 1, pp. 212–215, Jan. 2004.
- [28] H. Ditlbacher, J. R. Krenn, G. Schider, A. Leitner, and F. R. Aussenegg, "Two-dimensional optics with surface plasmon polaritons," *Appl. Phys. Lett.*, vol. 81, no. 10, pp. 1762–1764, Sep. 2002.
- [29] H. Ditlbacher, J. R. Krenn, A. Hohenau, A. Leitner, and F. R. Aussenegg, "Efficiency of local light-plasmon coupling," *Appl. Phys. Lett.*, vol. 83, no. 18, pp. 3665–3667, Nov. 2003.
- [30] R. Charbonneau, N. Lahoud, G. Mattiussi, and P. Berini, "Demonstration of integrated optics elements based on long-ranging surface plasmon polaritons," *Opt. Express*, vol. 13, no. 3, pp. 977–984, Feb. 2005.
- [31] T. Nikolajsen, K. Leosson, and S. I. Bozhevolnyi, "Surface plasmon–polariton based modulators and switches operating at telecom wavelengths," *Appl. Phys. Lett.*, vol. 85, no. 24, pp. 5833–5835, Dec. 2004.
- [32] J.-C. Weeber, Y. Lacroute, A. Dereux, E. Devaux, T. Ebbesen, C. Girard, M. U. Gonzalez, and A.-L. Baudrion, "Near-field characterization of Bragg mirrors engraved in surface plasmon waveguides," *Phys. Rev. B, Condens. Matter*, vol. 70, no. 23, pp. 235–406, Dec. 2004.
- [33] B. Prade, J. Y. Vinet, and A. Mysyrowicz, "Guided optical waves in planar heterostructures with negative dielectric constant," *Phys. Rev. B, Condens. Matter*, vol. 44, no. 24, pp. 13 556–13 572, Dec. 1991.
- [34] B. Temelkuran, S. D. Hart, G. Benoit, J. D. Joannopoulos, and Y. Fink, "Wavelength-scalable hollow optical fibers with large photonic bandgaps for CO₂ laser transmission," *Nature*, vol. 420, no. 6916, pp. 650–653, Dec. 2002.
- [35] M. A. Duguay, Y. Kokubun, T. Koch, and L. Pfeiffer, "Antiresonant reflecting optical waveguides in SiO₂–Si multilayer structures," *Appl. Phys. Lett.*, vol. 49, no. 1, pp. 13–15, Jul. 1986.
- [36] V. R. Almeida, Q. Xu, C. A. Barrios, and M. Lipson, "Guiding and confining light in void nanostructure," *Opt. Lett.*, vol. 29, no. 11, pp. 1209–1211, Jun. 2004.
- [37] T. W. Ebbesen, H. J. Lezec, H. F. Ghaemi, T. Thio, and P. A. Wolff, "Extraordinary optical transmission through sub-wavelength hole arrays," *Nature*, vol. 391, no. 12, pp. 667–669, Feb. 1998.
- [38] E. D. Palik, *Handbook of Optical Constants of Solids*, 2nd ed. San Diego, CA: Academic, 1998.
- [39] J. A. Dionne, L. A. Sweatlock, H. A. Atwater, and A. Polman, "Plasmon slot waveguides: Towards chip-scale propagation with subwavelength-scale localization," *Phys. Rev. B, Condens. Matter*, vol. 73, no. 3, p. 035 407, Jan. 2006.
- [40] S. K. Y. Kim, Y. K. Cho, H.-S. Tae, and J.-H. Lee, "Light transmission along dispersive plasmonic gap and its subwavelength guidance characteristics," *Opt. Express*, vol. 14, no. 1, pp. 320–330, Jan. 2006.
- [41] P. Ginzburg and M. Orenstein, "Plasmonic transmission lines: From micro to nano scale lambda/4 impedance matching," presented at the 1st European Topical Meeting Nanophotonics and Metamaterials, Tirol, Austria, 2007, Paper WED4f.60.
- [42] B. Wang and G. P. Wang, "Metal heterowaveguides for nanometric focusing of light," *Appl. Phys. Lett.*, vol. 85, no. 16, pp. 3599–3601, Oct. 2004.
- [43] J. Takahara, S. Yamagishi, H. Taki, A. Morimoto, and T. Kobayashi, "Guiding of a one-dimensional optical beam with nanometer diameter," *Opt. Lett.*, vol. 22, no. 7, pp. 475–477, Apr. 1997.

- [44] T. Takano and J. Hamasaki, "Propagating modes of a metal-clad-dielectric-slab waveguide for integrated optics," *IEEE J. Quantum Electron.*, vol. QE-8, no. 2, pp. 206–212, Feb. 1972.
- [45] J. A. Dionne, L. A. Sweatlock, H. A. Atwater, and A. Polman, "Planar metal plasmon waveguides: Frequency-dependent dispersion, propagation, localization, and loss beyond the free electron model," *Phys. Rev. B, Condens. Matter*, vol. 72, no. 7, p. 075405, Aug. 2005.
- [46] T. Goto, Y. Katagiri, H. Fukuda, H. Shinjima, Y. Nakano, I. Kobayashi, and Y. Mitsuoka, "Propagation loss measurement for surface plasmon-polariton modes at metal waveguides on semiconductor substrates," *Appl. Phys. Lett.*, vol. 84, no. 6, pp. 852–854, Feb. 2004.
- [47] M. P. Nezhad, K. Tetz, and Y. Fainman, "Gain assisted propagation of surface plasmon polaritons on planar metallic waveguides," *Opt. Express*, vol. 12, no. 17, pp. 4072–4079, Aug. 2004.
- [48] S. A. Maier, "Gain-assisted propagation of electromagnetic energy in subwavelength surface plasmon polariton gap waveguides," *Opt. Commun.*, vol. 258, no. 2, pp. 295–299, Feb. 2006.
- [49] P. Ginzburg, D. Arbel, and M. Orenstein, "Efficient coupling of nanoplasmonics to micro-photon circuitry," presented at the Conf. Lasers Electro-Optics/Quantum Electronics Laser Sci. Photonic Applications Syst. Technol., Baltimore, MD, 2005, Paper CWN5.
- [50] P. Ginzburg, D. Arbel, and M. Orenstein, "Gap plasmon polariton structure for very efficient microscale-to-nanoscale interfacing," *Opt. Lett.*, vol. 31, no. 22, pp. 3288–3290, Nov. 2006.
- [51] D. F. P. Pile and D. K. Gramotnev, "Adiabatic and nonadiabatic nanofocusing of plasmons by tapered gap plasmon waveguides," *Appl. Phys. Lett.*, vol. 89, no. 4, p. 041111, Jul. 2006.
- [52] G. Veronis and S. Fan, "Theoretical investigation of compact couplers between dielectric slab waveguides and two-dimensional metal-dielectric-metal plasmonic waveguides," *Opt. Express*, vol. 15, no. 3, pp. 1211–1221, Feb. 2007.
- [53] G. Veronis and S. Fan, "Bends and splitters in metal-dielectric-metal subwavelength plasmonic waveguides," *Appl. Phys. Lett.*, vol. 87, no. 13, p. 131102, Sep. 2005.
- [54] E. Feigenbaum and M. Orenstein, "Perfect 4-way plasmon splitting in cross gap waveguides intersection," presented at the IEEE/Laser and Electro-Optics Society Annu. Meeting (IEEE/LEOS), Montreal, QC, Canada, 2006, Paper WY5.
- [55] R. Zia, M. D. Selker, P. B. Catrysse, and M. L. Brongersma, "Geometries and materials for subwavelength surface plasmon modes," *J. Opt. Soc. Amer.*, vol. 21, no. 12, pp. 2442–2446, Dec. 2006.
- [56] Y.-F. Li and J. W. Y. Lit, "General formulas for the guiding properties of a multilayer slab waveguide," *J. Opt. Soc. Amer. A, Opt. Image Sci.*, vol. 4, no. 4, pp. 671–677, Apr. 1987.
- [57] Y. Satubi, I. Livne, A. Mashiach, D. Arbel, and M. Orenstein, *On the Dimensions of Surface-Plasmon-Polariton Waveguide—From Gap to Slab Guiding*. Personal communications, to be submitted.
- [58] A. A. Oliner and S. T. Peng, "Guidance and leakage properties of a class of open dielectric waveguides: Part II—New physical effects," *IEEE Trans. Microw. Theory Tech.*, vol. MTT-29, no. 9, pp. 855–869, Sep. 1981.
- [59] F. Kusunokia, T. Yotsuya, J. Takahara, and T. Kobayashi, "Propagation properties of guided waves in index-guided two-dimensional optical waveguides," *Appl. Phys. Lett.*, vol. 86, no. 21, p. 211101, May 2005.
- [60] G. Veronis and S. Fan, "Guided subwavelength plasmonic mode supported by a slot in a thin metal film," *Opt. Lett.*, vol. 30, no. 24, pp. 3359–3361, Dec. 2005.
- [61] K. Tanaka and M. Tanaka, "Simulations of nanometric optical circuits based on surface plasmon polariton gap waveguide," *Appl. Phys. Lett.*, vol. 82, no. 8, pp. 1158–1160, Feb. 2003.
- [62] K. Tanaka, M. Tanaka, and T. Sugiyama, "Simulation of practical nanometric optical circuits based on surface plasmon polariton gap waveguides," *Opt. Express*, vol. 13, no. 1, pp. 256–266, Jan. 2005.
- [63] R. Gordon and A. G. Brolo, "Increased cut-off wavelength for a subwavelength hole in a real metal," *Opt. Express*, vol. 13, no. 6, pp. 1933–1938, Mar. 2005.
- [64] Y. Satubi and M. Orenstein, "Surface-plasmon-polariton modes in deep metallic trenches—Measurement and analysis," *Opt. Express*, vol. 15, no. 7, pp. 4247–4252, Apr. 2007.
- [65] Y. Satubi and M. Orenstein, "Surface plasmon polariton waveguiding—From multi-mode stripe to a slot geometry," *Appl. Phys. Lett.*, vol. 90, no. 52, p. 251104, Jun. 2007.
- [66] D. F. P. Pile, T. Ogawa, D. K. Gramotnev, Y. Matsuzaki, K. C. Vernon, K. Yamaguchi, T. Okamoto, M. Haraguchi, and M. Fukui, "Two-dimensionally localized modes of a nanoscale gap plasmon waveguide," *Appl. Phys. Lett.*, vol. 87, no. 26, p. 261114, Dec. 2005.
- [67] L. Liu, Z. Han, and S. He, "Novel surface plasmon waveguide for high integration," *Opt. Express*, vol. 13, no. 17, pp. 6645–6650, Aug. 2005.
- [68] S. I. Bozhvolny, "Effective-index modeling of channel plasmon polaritons," *Opt. Express*, vol. 14, no. 20, pp. 9467–9476, Oct. 2006.
- [69] S. I. Bozhvolny, V. S. Volkov, E. Devaux, J. Y. Laluet, and W. Ebbesen, "Channel plasmon subwavelength waveguide components including interferometers and ring resonators," *Nature*, vol. 440, no. 23, pp. 508–511, Mar. 2006.
- [70] S. I. Bozhvolny, V. S. Volkov, E. Devaux, and W. Ebbesen, "Channel plasmon-polariton guiding by subwavelength metal grooves," *Phys. Rev. Lett.*, vol. 95, no. 4, p. 046802, Jul. 2005.
- [71] *Private Communications on Slot Lines Simulations*.
- [72] I. V. Novikov and A. A. Maradudin, "Channel polaritons," *Phys. Rev. B, Condens. Matter*, vol. 66, no. 3, p. 035403, Jun. 2002.
- [73] E. Moreno, F. J. Garcia-Vidal, S. G. Rodrigo, L. Martin-Moreno, and S. I. Bozhvolnyi, "Channel plasmon-polaritons: Modal shape, dispersion, and losses," *Opt. Lett.*, vol. 31, no. 23, pp. 3447–3449, Dec. 2006.
- [74] D. F. P. Pile and D. K. Gramotnev, "Channel plasmon-polariton in a triangular groove on a metal surface," *Opt. Lett.*, vol. 29, no. 10, pp. 1069–1071, May 2004.
- [75] D. F. P. Pile and D. K. Gramotnev, "Single-mode subwavelength waveguide with channel plasmon-polaritons in triangular grooves on a metal surface," *Appl. Phys. Lett.*, vol. 85, no. 26, pp. 6323–6325, Dec. 2004.
- [76] D. Arbel and M. Orenstein, "W-shaped plasmon waveguide for silicon based plasmonic modulator," presented at the IEEE/Laser Electro-Optics Soc. Annu. Meeting (IEEE/LEOS), Montreal, QC, Canada, 2006, Paper TuL5.
- [77] S. L. Chen, J. Shakyia, and M. Lipson, "Subwavelength confinement in an integrated metal slot waveguide on silicon," *Opt. Lett.*, vol. 31, no. 14, pp. 2133–2135, Jul. 2006.
- [78] D. F. P. Pile, T. Ogawa, D. K. Gramotnev, T. Okamoto, M. Haraguchi, M. Fukui, and S. Matsuo, "Theoretical and experimental investigation of strongly localized plasmons on triangular metal wedges for subwavelength waveguiding," *Appl. Phys. Lett.*, vol. 87, no. 6, p. 061106, Aug. 2005.
- [79] A. D. Boardman, G. C. Aers, and R. Teshima, "Retarded edge modes of parabolic wedge," *Phys. Rev. B, Condens. Matter*, vol. 24, no. 10, pp. 5703–5712, Nov. 1981.
- [80] J. Q. Lu and A. A. Maradudin, "Channel plasmons," *Phys. Rev. B, Condens. Matter*, vol. 42, no. 17, pp. 11159–11165, Dec. 1990.
- [81] L. Dobrzynski and A. A. Maradudin, "Electrostatic edge modes in a dielectric wedge," *Phys. Rev. B, Condens. Matter*, vol. 6, no. 10, pp. 3810–3815, Nov. 1972.
- [82] A. Eguiluz and A. A. Maradudin, "Electrostatic edge modes along a parabolic wedge," *Phys. Rev. B, Condens. Matter*, vol. 14, no. 12, pp. 5526–5528, Dec. 1976.
- [83] A. D. Boardman, R. Garcia-Molina, A. Gras-Marti, and E. Louis, "Electrostatic edge modes of a hyperbolic dielectric wedge: Analytic solution," *Phys. Rev. B, Condens. Matter*, vol. 32, no. 9, pp. 6045–6047, Nov. 1985.
- [84] E. Feigenbaum and M. Orenstein, "Nano plasmon polariton modes of a wedge cross section metal waveguide," *Opt. Express*, vol. 14, no. 19, pp. 8779–8784, Sep. 2006.
- [85] A. Karalis, E. Lidorikis, M. Ibanescu, J. D. Joannopoulos, and M. Soljacic, "Surface-plasmon-assisted guiding of broadband slow and subwavelength light in air," *Phys. Rev. Lett.*, vol. 95, no. 6, p. 063901, Aug. 2005.
- [86] H. T. Miyazaki and Y. Kurokawa, "Squeezing visible lightwaves into a 3-nm-thick and 55-nm-long plasmon cavity," *Phys. Rev. Lett.*, vol. 96, no. 9, p. 097401, Mar. 2006.
- [87] H. T. Miyazaki and Y. Kurokawa, "Metal-insulator-metal plasmon nanocavities: Analysis of optical properties," *Phys. Rev. B, Condens. Matter*, vol. 75, no. 3, p. 035411, Jan. 2007.
- [88] E. Feigenbaum and M. Orenstein, "Optical 3D cavity modes below the diffraction-limit using slow-wave surface-plasmon-polaritons," *Opt. Express*, vol. 15, no. 5, pp. 2607–2612, Mar. 2007.
- [89] P. Ginzburg, E. Feigenbaum, and M. Orenstein, "2D photonic band gap cavities embedded in a plasmonic gap structures—Zero model volume?" presented at the IEEE/Laser Electro-Optics Society Annu. Meeting (IEEE/LEOS), Sydney, Australia, 2005, Paper TuZ5.
- [90] L. C. Andreani, G. Panzarini, and J. M. Gérard, "Strong-coupling regime for quantum boxes in pillar microcavities: Theory," *Phys. Rev. B, Condens. Matter*, vol. 60, no. 19, pp. 13276–13279, Nov. 1999.
- [91] E. Feigenbaum and M. Orenstein, "Plasmon-soliton," *Opt. Lett.*, vol. 32, no. 6, pp. 674–676, Mar. 2007.



Eyal Feigenbaum was born in Haifa, Israel. He received the B.Sc. and M.Sc. degrees from Technion—Israel Institute of Technology, Haifa, in 1998 and 2004, respectively. He is currently working toward the Ph.D. degree in electrical engineering at Technion.

His current research interests include optical plasmonics and nonlinear optics, as well as spatial and temporal solitons.



Meir Orenstein was born in Haifa, Israel. He received the B.Sc. and Ph.D. degrees from the Technion—Israel Institute of Technology, Haifa.

Since 1991, he has been a Professor of electrical engineering with Technion, where he is the Head of the Micro-photonics Laboratory and a member of the Micro/Nano-electronics Center, Opto-electronics Center, Center of Communications and Information Technology, and Technion's Asher Space Institute. Previously, he was a Scientist with Bellcore and was the Chief Scientist of the R&D branch of El-Op, which is Israel's leading electrooptic company. He is the Cofounder of Lambda Crossing and Optun, which are startup companies in the field of optically integrated switches and tunable filters. His research interests include theoretical and experimental investigation of microcavities, vertical cavity diode lasers and arrays, emission of photons with orbital angular momentum, spatial and temporal optical solitons, photonic circuitry, optical plasmonics, metamaterials, nonreversal optics, optical interconnects, and quantum communications.